Simple Representations of Zero-Net Mass-Flux Jets in Grazing Flow for Flow-Control Simulations

by

Ehsan Aram, Rajat Mittal and Louis Cattafesta

Reprinted from

International Journal of
Flow Control

Volume 2 · Number 2 · June 2010

Multi-Science Publishing
ISSN 1756-8250

Simple Representations of Zero-Net Mass-Flux Jets in Grazing Flow for Flow-Control Simulations

Ehsan Aram,[1] Rajat Mittal[2]
Department of Mechanical Engineering,
Johns Hopkins University, Baltimore, MD - 21218

and

Louis Cattafesta[3]
Interdisciplinary Microsystems Group
Department of Mechanical and Aerospace Engineering,
University of Florida, Gainesville, FL - 32611

Simple boundary conditions that can represent the flow emanating from zero-net mass-flux (ZNMF) jets in grazing flows are examined. Two-dimensional Navier-Stokes simulations of ZNMF jets in grazing flow are used to determine the key characteristics of the jet profile, and these are used to construct a series of boundary condition models. These boundary condition models are then tested for a jet emanating into an attached boundary layer as well as a boundary layer with an induced separation bubble. A key finding of the current study is that simple plug-flow type models of ZNMF jets can lead to incorrect trends in separation control. Based on this analysis, we select two models that are simple, yet provide a reasonable representation of the ZNMF jet in a grazing flow. An empirical closure of these models is also suggested.

NOMENCLATURE

C_{uu} = u momentum flux in x-direction
C_{uv} = u momentum flux in y-direction
$\overline{C_{uv}}$ = Time average of C_{uv}
C_{vu} = v momentum flux in x-direction
C_{vv} = v momentum flux in y-direction
$\overline{C_{vv}}$ = Time average of C_{vv}
C_{vvv} = Vertical kinetic energy flux in y-direction
$\overline{C_{vvv}}$ = Time average of C_{vvv}
d = Slot width
F^+ = Dimensionless forcing frequency, f_J/f_{Sep}
f_J = Forcing frequency of ZNMF jet
f_{Sep} = Separation bubble frequency
H = Cavity height
h = Slot height
Q = Volume flow rate of ZNMF jet
Q_1 = Volume flow rate amplitude of ZNMF jet
Re_δ = Boundary layer Reynolds number, $U_\infty \delta/\nu$
Re_J = Jet Reynolds number, $\overline{V}_J\, d/\nu$
S = Stokes number, $\sqrt{\omega d^2/\nu}$

[1] Graduate Student, Department of Mechanical Engineering, earam1@jhu.edu

[2] Professor, Department of Mechanical Engineering, mittal@jhu.edu

[3] Professor, Department of Mechanical & Aerospace Engineering, cattafes@ufl.edu

St = Strouhal number, $2\pi fd / \overline{V_J}$
U_i = Fourier expansion amplitudes of u-velocity along the slot exit, $i = 0, 1, 2, \ldots$
$\overline{U_0}$ = Time average of U_0 over the expulsion phase
U_∞ = Free stream velocity
u = Streamwise velocity (in x-direction)
$\overline{u}$ = Time average of u-velocity
V_J = Spatial average of jet v-velocity along the slot exit
$\overline{V_J}$ = Time average of V_J during the expulsion phase
V_J^L = Spatial average of jet v-velocity along left half of the slot exit
$\overline{V_J^L}$ = Time average of V_J^L over the expulsion phase
V_J^R = Spatial average of jet v-velocity along right half of the slot exit
$\overline{V_J^R}$ = Time average of V_J^R over the expulsion phase
$V_i^{(2)}$ = Fourier expansion amplitudes of V_J^L, $i = 0, 1, 2, \ldots$
$V_i^{(3)}$ = Fourier expansion amplitudes of V_J^R, $i = 0, 1, 2, \ldots$
v = Cross-stream velocity (in y-direction)
W = Cavity width
x = Horizontal direction
y = Vertical direction
δ = Boundary layer thickness
ξ_z = Spanwise vorticity
Ω = Spanwise vorticity flux
$\overline{\Omega}$ = Time average of Ω
ν = Kinematic viscosity
ω = Angular forcing frequency of the ZNMF jet, $2\pi f_J$

I. INTRODUCTION

Zero-net mass-flux (ZNMF) or synthetic jet actuators are versatile devices with numerous applications including active control of flow separation, mixing enhancement, heat transfer, and thrust vectoring of jets.[1-4] A number of parametric studies indicate that several geometrical and flow parameters govern the performance characteristics of ZNMF jets and their control effectiveness.[5-7] The scales of these jets may be $10^{-2} - 10^{-3}$ times smaller in size compared to the dominant length scale of the problem (such as the wing chord). Thus, conducting numerical flow simulations which include full representations of the actuator cavity and/or slot is an extremely daunting proposition.[8] A more attractive approach is to devise a simpler representation of the actuator and use that instead of simulating the full actuator.

A variety of such approaches have been used in the past. For instance, Kral *et al.*[9] simulated the jet flow associated with a two-dimensional, incompressible synthetic jet actuator in the quiescent external flow by prescribing modified boundary conditions for velocity and pressure at the jet exit. Comparison between the computational results and experimental data for both steady and unsteady conditions showed good agreement in the turbulent case, but the model was not able to capture the breakdown of the vortex train in the laminar case. Rizzetta *et al.*[10] used the recorded jet exit velocity profile of an isolated actuator as the boundary condition for the 2D and 3D external flow field.

Other more sophisticated approaches have also been used with varying degrees of success. Filz *et al.*[11] have modeled 2D isolated synthetic jets as well as a synthetic jet in grazing flow using deterministic source terms trained by a neural network. The source terms were calculated from the time-average of the unsteady solution. This technique was able to reduce the computational time significantly and predict the momentum thickness of the flow with reasonable accuracy. A low-dimensional model of 2D and 3D synthetic jet actuator based on the unsteady compressible quasi-one-dimensional Euler equations was proposed by Yamaleev and Carpenter[12] and tested in grazing flow. Their model satisfied the conservation laws and was able to predict the resonance characteristics of the actuator. Although this model reduced the computational cost by eliminating the cavity, it did not consider the effects associated with the vortex generation, boundary layer, and the boundary-layer separation inside the actuator cavity.

With regards to simplified actuator models, Rathnasingham and Breuer[13] developed a system of first-order, non-linear differential equations which represented the fluid structure-interaction characteristics of the device in a quiescent external flow. The membrane was modeled as a circular plate, and the Bernoulli equation was used for flow in the slot. Comparison with experimental data showed that the semi-empirical model could accurately predict the time and frequency characteristics of the jet. Gallas *et al.*[5] and Agashe *et al.*[14] have developed lumped-element models (LEM) of piezoelectric and electrodynamic actuators in the quiescent external flow, respectively. In this approach, each component of the actuator is modeled as an element of an equivalent electrical circuit. Comparisons with the experimental results of prototype actuators reveal good agreement, but this method is incapable of providing detailed profiles of the flow quantities at the slot/orifice exit. Motivated by the LEM, Ravi[15] used numerical simulations to explore the idea of replacing the ZNMF jet in grazing flow with appropriately selected boundary conditions applied on the surface. He compared the simpler model with full simulations that included the cavity and slot. Several candidate profiles were considered. The overall conclusion was that none of these simple models were able to produce the effect of the jet on the cross flow boundary layer. Tang *et al.*[16] have recently predicted the instantaneous spatially average velocity at the orifice exit of a synthetic jet in quiescent flow by three different models which they call the dynamic incompressible flow model, the static compressible flow model and the (traditional) LEM. Comparisons with the experimental and numerical results suggested that the LEM model performs more reliably than the static compressible flow model in different conditions. A simple "slot only" model based on including only the jet slot (and not the cavity) of the actuator in grazing flow has also recently been proposed by Raju *et al.*[8] Comparison with the full cavity and a simple sinusoidal plug flow velocity model showed that this simplified actuator model was able to capture more of the flow physics associated with the full cavity simulations and could more accurately predict the reduction of the separation bubble size for a induced flow separation.

Although the ''slot-only" model represents a significant reduction in the computational complexity required to represent the actuator in flow simulations, it still requires simulation of the unsteady viscous flow in the slot. Furthermore, if the slot location is varied, a new grid may have to be generated. If, however, the entire actuator can be replaced by an appropriate and relatively simple velocity boundary condition at the jet exit, there would be no need to include a slot, and that would significantly simplify the task of ZNMF flow control simulations. In the current paper, we explore the possibility of developing just such a boundary condition representation for ZNMF jets in grazing external flow.

II. MODIFIED BOUNDARY CONDITION ACTUATOR MODELS

The approach taken in the current study is to use the jet exit profile of a full cavity simulation (i.e. a simulation where the jet actuator cavity and slot are explicitly included) to construct a simple low-order description of the ZNMF jet. An attempt is made to reproduce the flow physics associated with the full cavity simulations using our proposed models. Since in the current study the oscillation frequency of the diaphragm is considered well below the Helmholtz frequency of the actuator, the incompressible flow assumption is fairly accurate inside the actuator and flow rate at the slot exit is directly proportional to the volume displacement of the diaphragm or piston that drives the flow. Utturkar *et al.*[17] showed that in the case of incompressible flow, the cavity shape has a very limited effect on the jet exit flow and we therefore assume a simple geometric model for the actuator. In cases where compressibility effects inside the cavity cannot be ignored, the volume flux is certainly affected by the cavity shape but can be predicted by lumped-element type models.[5, 14] However, regardless of whether the flow inside the cavity behaves in a compressible or incompressible manner, the details of the jet profile and the momentum/energy flux from the jet, for a given jet volume flux, depend primarily on characteristics of the flow through the slot as well as the grazing flow. The current effort is directed towards modeling these effects.

Figure 1(a) & (b) show a schematic of the two configurations considered in the current study: the Full Cavity (FC) and the Modified Boundary Condition (MBC) models. As it is seen in Fig. 1(a), the actuator diaphragm is located at the bottom of the cavity, and a sinusoidal plug flow profile on the bottom wall is prescribed to model the effect of diaphragm motion on the flow. In the current study, the FC model is considered as the "gold standard", and the objective of the current study is to assess a variety of MBC models by comparing with the FC model.

By far the simplest MBC model is one that assumes a sinusoidally varying plug flow for the vertical velocity profile at the jet exit during the expulsion and ingestion phase. Numerical simulations also

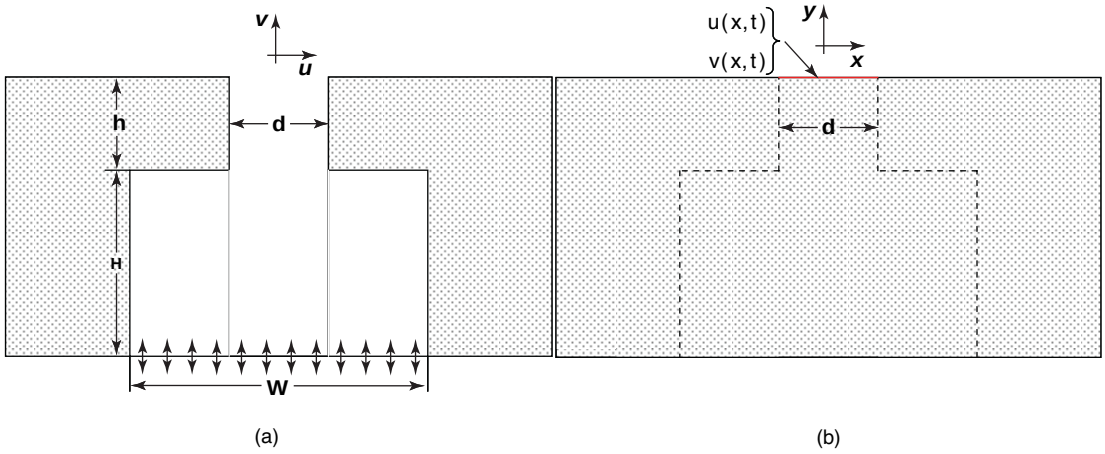

Figure 1: Schematic of (a) full cavity (FC) and (b) modified boundary condition (MBC) model.

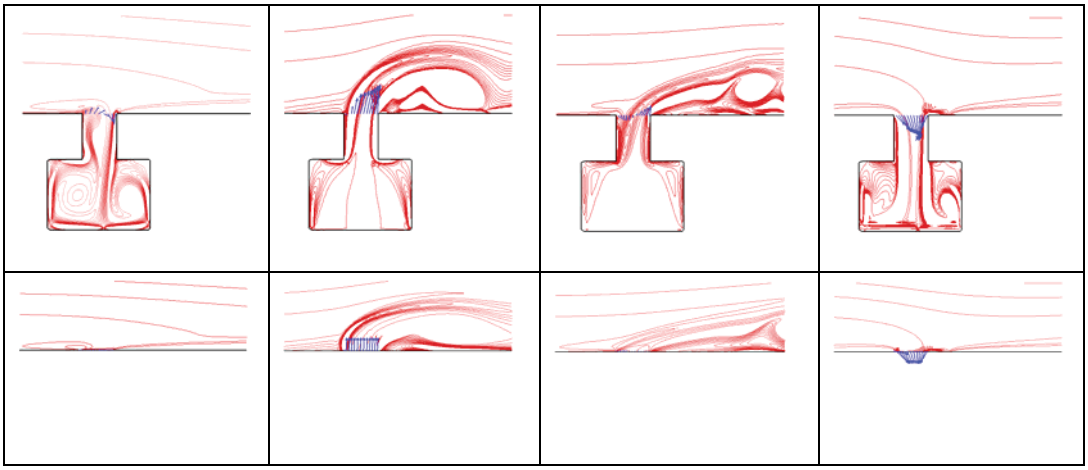

Figure 2: Velocity vectors and instantaneous spanwise vorticity contours for the full cavity (top row) and MBC1 (bottom row) models at four different phases $\varphi = 0°$, 90°, 180°, 270°. The plots are for a case with $\mathrm{Re}_J = 250$, $S = 7.07$, $St = 0.2$, $U_\infty/\overline{V_J} = 4$ and $\delta/d = 3$.

require the specification of the horizontal velocity component in this simplest MBC model. Our past studies (Raju *et al.*[8]) have shown that, assuming a zero Neumann boundary condition for the horizontal velocity u during the ingestion phase is essential for numerical stability, and so that is the condition employed for the horizontal velocity component during the ingestion phase. Generally, this simple model assumes that the horizontal velocity is zero during the expulsion phase and the amplitude of the vertical velocity is chosen so as to match the volume flux of the FC model. We denote this model as MBC1. In Fig. 2, we compare the instantaneous spanwise vorticity contours produced by the FC model to that of the MBC1 model for a case where the jet is emanating into a grazing laminar boundary layer. The dimensionless flow parameters for this comparison are $\mathrm{Re}_J = 250$, $St = 0.2$, $U_\infty/\overline{V_J} = 4$ and $\delta/d = 3$. A comparison of the external flow and the jet exit velocity profile suggests the following. First, the simple MBC1 type model produces an external flow that is different from that of the FC model, especially during the expulsion phase. Second, the vertical velocity shows significant variations along the slot width. Third, the flow at the slot exit has a non-zero horizontal velocity component which could potentially have an important effect on the jet. We use these observations as a basis for exploring a set of MBC models in the following section.

Two key factors need to be considered while designing viable MBC models for ZNMF jets in grazing flows. First, the models should be as simple as possible and have a relatively small number of parameters. Second, the model should provide a reasonably good approximation to the effects of the actual ZNMF jet. Keeping this in mind, we introduce models which have at most two spatial degrees

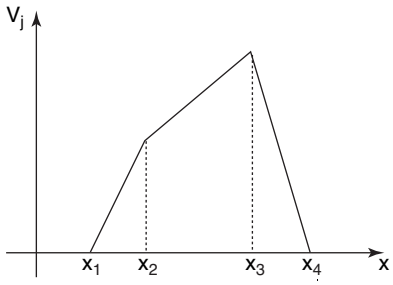

Figure 3: Assumed vertical velocity profile for MBC models.

of freedom for the vertical velocity. We prescribe the vertical velocity for at most two interior points across the slot exit. This allows us to prescribe a non-uniform velocity profile across the slot. Furthermore at any given time, we assume a linear velocity variation between these two points and impose the no-slip boundary condition at the slot edges. Figure 3 shows the type of vertical velocity profile that is employed in our MBC models where (2) and (3) are the points where the velocity is specified and points (1) and (4) are the slot edge points. The points (2) and (3) can in principle be located anywhere, but we choose a simple prescription whereby the points are located at 25% and 75% locations along the slot exit. With regards to the horizontal velocity component, in the interest of simplicity, we assume that there is no spatial variation of this component of velocity during the expulsion phase. Note that the no-slip boundary condition is imposed at the slot edges for horizontal velocity during the expulsion and ingestion phases. We denote the vertical velocity at the points (2) and (3) as $V_J^{(2)}$ and $V_J^{(3)}$, respectively, and the horizontal velocity as U_J.

The next consideration is the time variation of this assumed profile for $V_J^{(2)}$, $V_J^{(3)}$ and V_J. We first assume that the volume flux through the slot is sinusoidal, i.e.

$$Q(t) = Q_1 \sin(\omega t) \tag{1}$$

Given this, it is natural to assume that the velocity at any given point across the jet slot is also periodic and can be expressed in terms of a Fourier series in time as follows:

$$\begin{aligned} V_J^{(2)}(t) &= V_0^{(2)} + V_1^{(2)} \sin(\omega t + \varphi_1^{(2)}) + V_1^{(2)} \sin(2\omega t + \varphi_2^{(2)}) + \cdots \\ V_J^{(3)}(t) &= V_0^{(3)} + V_1^{(3)} \sin(\omega t + \varphi_1^{(3)}) + V_2^{(3)} \sin(2\omega t + \varphi_2^{(3)}) + \cdots \\ U_J(t) &= U_0 + U_1 \sin(\omega t + \psi_1) + U_2 \sin(2\omega t + \psi_2) + \cdots \end{aligned} \tag{2}$$

Based on conservation of mass we obtain the following relationships for the above coefficients:

$$V_0^{(2)} = -V_0^{(3)} = V_0 \tag{3}$$

We now look at the FC model for guidance regarding the amplitudes and phases of the terms in the above Fourier series. Figure 4(a) shows the velocity averaged over the right and left halves of the slot exit as well as the average velocity over the entire slot (which is an exact sinusoid). These are computed as:

$$V_J^L(t) = \frac{2}{d}\int_0^{d/2} v(x,t)dx; \quad V_J^R(t) = \frac{2}{d}\int_{d/2}^{d} v(x,t)dx; \quad \text{and} \quad V_J(t) = \frac{1}{d}\int_0^{d} v(x,t)dx \tag{4}$$

If we assume that $V_J^{(2)}$ and $V_J^{(3)}$ are related to V_J^L and V_J^R respectively, we find from Fig. 4(a) that $V_J^{(2)}$ and $V_J^{(3)}$ vary mostly at the ZNMF jet frequency implying that higher harmonics are negligible, i.e.

$$V_1^{(2)} \gg V_n^{(2)} \quad for \;\; n > 1 \tag{5a}$$

$$V_1^{(3)} \gg V_n^{(3)} \quad for \;\; n > 1 \tag{5b}$$

Second, the two velocities are also approximately in phase with the volume flux, suggesting that

$$\phi_1^{(2)}, \phi_1^{(3)} \approx 0 \tag{6}$$

Next, Fig. 4(b) shows the spatial average of the horizontal u velocity component at the exit of the full cavity over one cycle. The spatial integral is calculated over the whole length of the exit. Two observations can be made from this plot. First, the time-space averaged horizontal velocity is non-zero. Second, the horizontal velocity component possesses a large Fourier amplitude at the first super harmonic of the jet frequency, i.e. 2ω with $\psi_2 \approx 0$.

Given all of the above observations, the following reduced representation of the velocity components can be obtained for the two interior points in the slot:

$$\begin{aligned} V_J^{(2)}(t) &= V_0 + V_1^{(2)} \sin(\omega t) \\ V_J^{(3)}(t) &= -V_0 + V_1^{(3)} \sin(\omega t) \\ U_J(t) &= U_0 + U_2 \sin(2\omega t) \end{aligned} \tag{7}$$

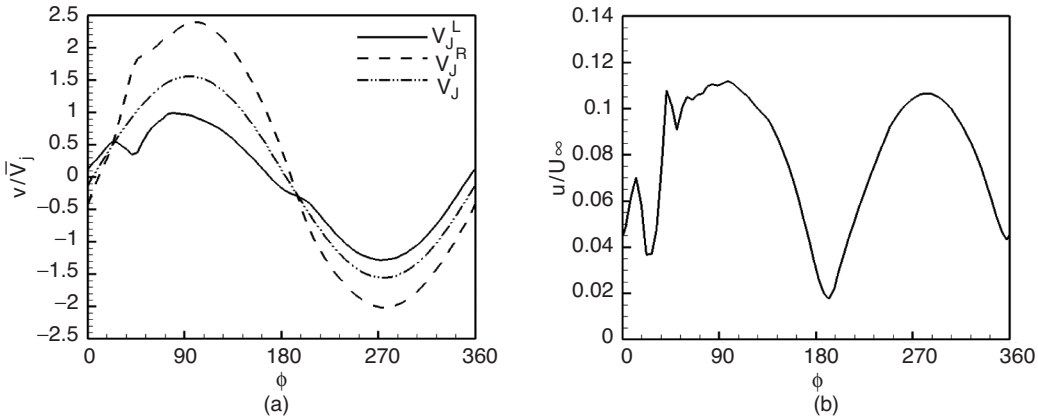

Figure 4: The spatial average of the jet velocity component along the slot exit of the full cavity model, (a) vertical v component of velocity, (b) horizontal u component of velocity.

Note that the above prescription has five coefficients. However, since $V_J^{(2)}$ and $V_J^{(3)}$ are related to the amplitude of the volume flux Q_1 over the expulsion phase, only four of these coefficients are unknown. In order to assess the viability of the above prescription (as well as further simplifications to it) we have evaluated the four remaining coefficients from the FC model. This is done by extracting the velocity components at the slot exit as a function of space and time from the FC simulations, evaluating the spatial average of velocity along the slot exit for horizontal velocity and along each half of slot separately for vertical velocity and then subjecting these to a Fourier analysis. For instance, $V_J^{(2)}$ is evaluated as the spatial average of the jet exit velocity on the left half of the slot, whereas $V_J^{(3)}$ is the corresponding velocity for the right half of the slot. We then create a number of variations of the above model by making further simplifying assumption(s) and compute the flows for these simpler models. The computed flows are then compared with the FC model to assess the performance of each model.

Proposed Models

Two key considerations in model development are fidelity and complexity. Model complexity is usually directly related to the number of unknowns in the model that require "closure". While the simplest models usually tend to be the ones with the lowest fidelity, increase in complexity beyond a certain stage is not necessarily accompanied by a corresponding increase in fidelity. The objective of the exercise below is to identify models that are relatively simple, yet provide significant improvement in fidelity over the simplest plug-flow model.

It should be pointed out that in general, expulsion and ingestion need to be treated separately in these models. This is because expulsion and ingestion for the jet represent inflow and outflow respectively for the computational domain, and numerical stability requires different treatments for these two

Table 1: Different modified boundary condition (MBC) models examined in current study.

Model	Expulsion	Ingestion	Unknowns	Remarks
MBC1	$U_J(t) = 0.0$ $V_J^{(2)}(t) = V_1^{(2)} \sin(\omega t)$ $V_J^{(3)}(t) = V_1^{(3)} \sin(\omega t)$ $V_1^{(2)} = V_1^{(3)} = Q_1/d$	$\partial u/\partial y = 0$ $V_J^{(2)}(t) = V_1^{(2)} \sin(\omega t)$ $V_J^{(3)}(t) = V_1^{(3)} \sin(\omega t)$ $V_1^{(2)} = V_1^{(3)} = Q_1/d$	None	• Plug flow model. • Zero u-vel during the expulsion phase. • Uniform v-vel. during the expulsion and ingestion phases. • Simplest model.
MBC2	$U_J(t) = 0.0$ $V_J^{(2)}(t) = V_0 + V_1^{(2)} \sin(\omega t)$ $V_J^{(3)}(t) = -V_0 + V_1^{(3)} \sin(\omega t)$ $V_1^{(2)} \neq V_1^{(3)}$	$\partial u/\partial y = 0$ $V_J^{(2)}(t) = V_0 + V_1^{(2)} \sin(\omega t)$ $V_J^{(3)}(t) = -V_0 + V_1^{(3)} \sin(\omega t)$ $V_1^{(2)} \neq V_1^{(3)}$	V_0 $\frac{V_1^{(3)}}{V_1^{(2)}}$	• u-vel same as MBC1. • Nonuniform v-vel amplitude with non zero mean value in left and right half of slot (phase difference) during the expulsion and ingestion phases.
MBC3	$U_J(t) = U_0 + U_2 \sin(2\omega t)$ $V_J^{(2)}(t) = V_0 + V_1^{(2)} \sin(\omega t)$ $V_J^{(3)}(t) = -V_0 + V_1^{(3)} \sin(\omega t)$ $V_1^{(2)} \neq V_1^{(3)}$	$\partial u/\partial y = 0$ $V_J^{(2)}(t) = V_0 + V_1^{(2)} \sin(\omega t)$ $V_J^{(3)}(t) = -V_0 + V_1^{(3)} \sin(\omega t)$ $V_1^{(2)} \neq V_1^{(3)}$	U_0 U_2 V_0 $\frac{V_1^{(3)}}{V_1^{(2)}}$	• Sinusoidal u-vel. with non zero mean value in expulsion phase. • v-vel. same as MBC2. • Most general model.
MBC4	$U_J(t) = U_0 + U_2 \sin(2\omega t)$ $V_J^{(2)}(t) = V_0 + V_1^{(2)} \sin(\omega t)$ $V_J^{(3)}(t) = -V_0 + V_1^{(3)} \sin(\omega t)$ $V_1^{(2)} \neq V_1^{(3)}$	$\partial u/\partial y = 0$ $V_J^{(2)}(t) = V_0 + V_1^{(2)} \sin(\omega t)$ $V_J^{(3)}(t) = -V_0 + V_1^{(3)} \sin(\omega t)$ $V_1^{(2)} = V_1^{(3)} = Q_1/d$	U_0 U_2 V_0 $\frac{V_1^{(3)}}{V_1^{(2)}}$	• u-vel. same as MBC3. • v-vel. same as MBC3 during the expulsion phase. • Uniform v-vel. amplitude with non zero mean value in left and right half of slot during the ingestion phase.
MBC5	$U_J(t) = U_0 + U_2 \sin(2\omega t)$ $V_J^{(2)}(t) = V_1^{(2)} \sin(\omega t)$ $V_J^{(3)}(t) = V_1^{(3)} \sin(\omega t)$ $V_1^{(2)} \neq V_1^{(3)}$	$\partial u/\partial y = 0$ $V_J^{(2)}(t) = V_1^{(2)} \sin(\omega t)$ $V_J^{(3)}(t) = V_1^{(3)} \sin(\omega t)$ $V_1^{(2)} = V_1^{(3)} = Q_1/d$	U_0 U_2 $\frac{V_1^{(3)}}{V_1^{(2)}}$	• u-vel. same as MBC4. • v-vel. same as MBC4 with zero mean value in both halves of slot during the expulsion phase. • v-vel. same as MBC1 during ingestion phase.
MBC6	$U_J(t) = U_0$ $V_J^{(2)}(t) = V_1^{(2)} \sin(\omega t)$ $V_J^{(3)}(t) = V_1^{(3)} \sin(\omega t)$ $V_1^{(2)} \neq V_1^{(3)}$	$\partial u/\partial y = 0$ $V_J^{(2)}(t) = V_1^{(2)} \sin(\omega t)$ $V_J^{(3)}(t) = V_1^{(3)} \sin(\omega t)$ $V_1^{(2)} = V_1^{(3)} = Q_1/d$	U_0 $\frac{V_1^{(3)}}{V_1^{(2)}}$	• Constant u-vel. in expulsion phase. • v-vel. same as MBC5.
MBC7	$U_J(t) = 0.0$ $V_J^{(2)}(t) = V_1^{(2)} \sin(\omega t)$ $V_J^{(3)}(t) = V_1^{(3)} \sin(\omega t)$ $V_1^{(2)} \neq V_1^{(3)}$	$\partial u/\partial y = 0$ $V_J^{(2)}(t) = V_1^{(2)} \sin(\omega t)$ $V_J^{(3)}(t) = V_1^{(3)} \sin(\omega t)$ $V_1^{(2)} = V_1^{(3)} = Q_1/d$	$\frac{V_1^{(3)}}{V_1^{(2)}}$	• u-vel. same as MBC1. • v-vel. same as MBC6.

situations. In particular, Dirichlet boundary conditions on all components of velocity cannot be imposed at an outflow boundary in regions where there is significant flux of vorticity since doing so leads to numerical instability. An acceptable treatment during ingestion therefore is to impose Dirichlet boundary conditions on the vertical component of velocity and homogeneous Neumann conditions on the horizontal component.

Table 1 lists the proposed models studied in this paper. We start with the simplest model (MBC1) and improve the model by adding the nonuniformity to the vertical velocity over the entire cycle (MBC2) and also prescribing the time-dependent horizontal velocity in expulsion phase in MBC3 (The most general and complex model), and for the rest of models, we try to simplify the MBC3 by removing unknowns and examine to what extent this simplification can influence the fidelity of the results. Note that for MBC5-7, a uniform vertical velocity profile is used during the ingestion phase.

Note that in the above profiles, if $V_1^{(2)} = V_1^{(3)}$ then we have the so-called "plug" flow profile wherein the vertical velocity is uniform across the slot exit at all time instants. Conversely, for models with $V_1^{(2)} \neq V_1^{(3)}$, we assume a non-uniform exit velocity profile. For models with $V_0 = 0$ we are assuming that both halves of the jet slot separately satisfy the zero-net mass-flux constraint.

The simulations to study the performance of the different models in the vicinity of the actuator have been carried out on the domain size of 28 $d \times 29.3\ d$ with a single grid of dimensions 257×161 for the MBCs, and a domain size of 28 $d \times 32\ d$ with a 257×257 grid for the full cavity model. In all models, 25 grid points are used along the jet exit. These grids are based on the previous simulations of Raju *et al.*[8,18] which were carried out over a wide range of flow parameters ($\mathrm{Re}_J = 93.75 - 500$, $S = 5 - 50$, $\delta/d = 0 - 3$, $U_\infty/\overline{V_J} = 0 - 4$), and subjected to grid refinement and domain dependency studies. The geometrical and flow parameters in the current work are also chosen based on this previous work. The geometrical parameters for the full cavity are $h/d = 1.0$, $W/d = 3.0$ and $H/d = 1.5$ (defined in Fig. 1). The values of the dimensionless flow parameters for the simulations are $\delta/d = 3.0$, $U_\infty/\overline{V_J} = 4$, $\mathrm{Re}_J = 250$ ($\mathrm{Re}_\delta = 3000$), $S = 7.07$ and $St = 0.2$.

The incompressible Navier–Stokes equations are discretized using a cell-centred, collocated arrangement of the primitive variables. The solver employs a second-order Adams-Bashforth scheme for the convective terms and an implicit Crank-Nicolson scheme for diffusion terms on a Cartesian grids. A second-order fractional step method is applied to solve the equations in time. The solver has been tested extensively by comparisons with the established numerical and experimental data including ZNMF jets.[19,20]

Canonical Separated Flow Configuration

One way to study the performance of potential models is to examine the effect of some of these models on a separated flow and understand to what extent the details of the actuator model are necessary to model the effects of the ZNMF jet on the separation bubble. In order to address this issue we have examined a case where a separation bubble is created downstream of the jet by prescribing a steady blowing-suction boundary condition on the top boundary of the domain. A zero-vorticity condition[21] is applied on this boundary as follows:

$$v(x, L_y) = G(x), \qquad \left.\frac{\partial u}{\partial y}\right|_{(x,\, L_y)} = \frac{dG}{dx} \tag{8}$$

where $G(x)$ is the prescribed blowing and suction velocity profile defined in the form of:

$$G(x) = -V_{top} \sin\left(\frac{2\pi(x - x_c)}{L}\right) e^{-\alpha\left\{\frac{2(x-x_c)}{L}\right\}^{\beta}} \tag{9}$$

where L is the length and x_c is the center of the velocity profile. The parameters V_{top}, α and β are set to U_∞, 10 and 20, respectively, which form a closed separation bubble on the flat plate. A schematic of the flow configuration is shown in Fig. 5. The inflow is a cubic approximation to the Blasius boundary layer

$$\frac{u}{U_\infty} = \frac{3}{2}\frac{y}{\delta} - \frac{1}{2}\left(\frac{y}{\delta}\right)^3 \tag{10}$$

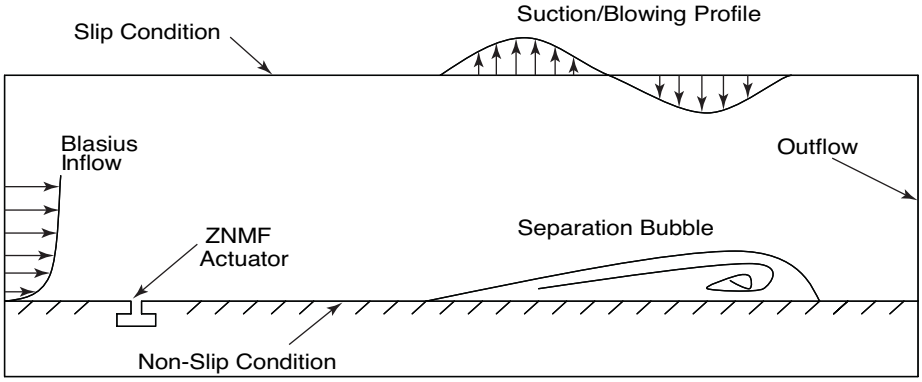

Figure 5: Flow configuration used for simulating a canonical separated flow.

Separated flow simulations have been performed for the following dimensionless flow parameters: $\delta/d = 3$, $U_\infty/\overline{V_J} = 4$, $\mathrm{Re}_J = 187.5, 250$ ($\mathrm{Re}_\delta = 2250, 3000$), and three dimensionless forcing frequencies $F^+ = 0.5, 1.0, 1.5$, where F^+ is the ratio of the jet frequency (f_J) to the dominant frequency in the separation bubble (f_{Sep}). We have used a 641×257 grid on the domain size of $96\,d \times 29\,d$ for MBC1 (plug flow), MBC6 and MBC7 models, and a domain size of $96\,d \times 32\,d$ with a 641×321 grid for the FC model. In all models, 12 grid points are used across the jet exit. These grids have been used before for ZNMF jet studies[8,18] and are known to provide adequate solution of the flow. Note that in this component of the study, all of the unknowns in the MBC models are obtained from FC model in external flow with no separation bubble (part A).

III. RESULTS

Model Performance in Vicinity of Actuator

Based on the criterion suggested by Holman *et al.*[7] a strong jet is formed for the current case with $St = 0.2$ and it is able to influence the boundary layer at a large distance in the streamwise direction and impart a significant amount of the spanwise vorticity flux to the external flow. Figure 6 shows a comparison of the spanwise vorticity at the peak expulsion for all of the models at the following condition: $\mathrm{Re}_J = 250$, $S = 7.07$, $St = 0.2$, $U_\infty/\overline{V_J} = 4$ and $\delta/d = 3$. The strength of the vortex at both edges of the slot exit in MBC1 (plug flow) is much less than the full cavity model, but the rest of the models provides a reasonable qualitative approximation to the full cavity model. Similar comparisons exist at other phases of the jet cycle.

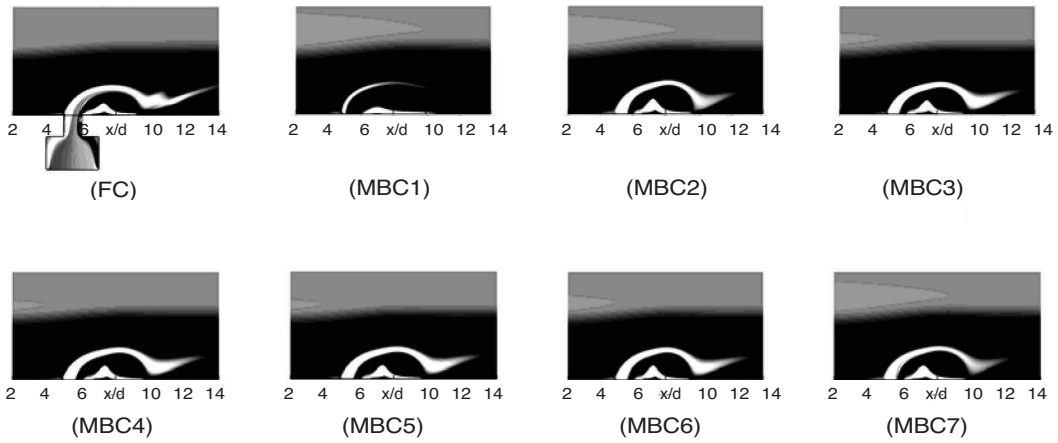

Figure 6: Instantaneous spanwise vorticity during peak expulsion.

The performance of these models can also be assessed based on the integral quantities such as average flux of spanwise vorticity, u and v momentum and vertical kinetic energy at the jet exit. The definitions for these quantities are as follows:

$$C_{uv}(t) = \rho \int_0^d u(x, t)v(x, t)dx; \quad C_{vv}(t) = \rho \int_0^d u(x, t)v(x, t)dx;$$

$$C_{vv}\, v(t) = \rho \int_0^d v^2(x, t)v(x, t)dx \quad \text{and} \quad \Omega(t) = \int_0^d |\xi_z(x, t)|v(x, t)dx \tag{11}$$

where $\xi_z(x, t)$ is the spanwise vorticity at the jet exit. The non-dimensionalized variation of these quantities over one jet cycle is compared for the various proposed models in Fig. 7.

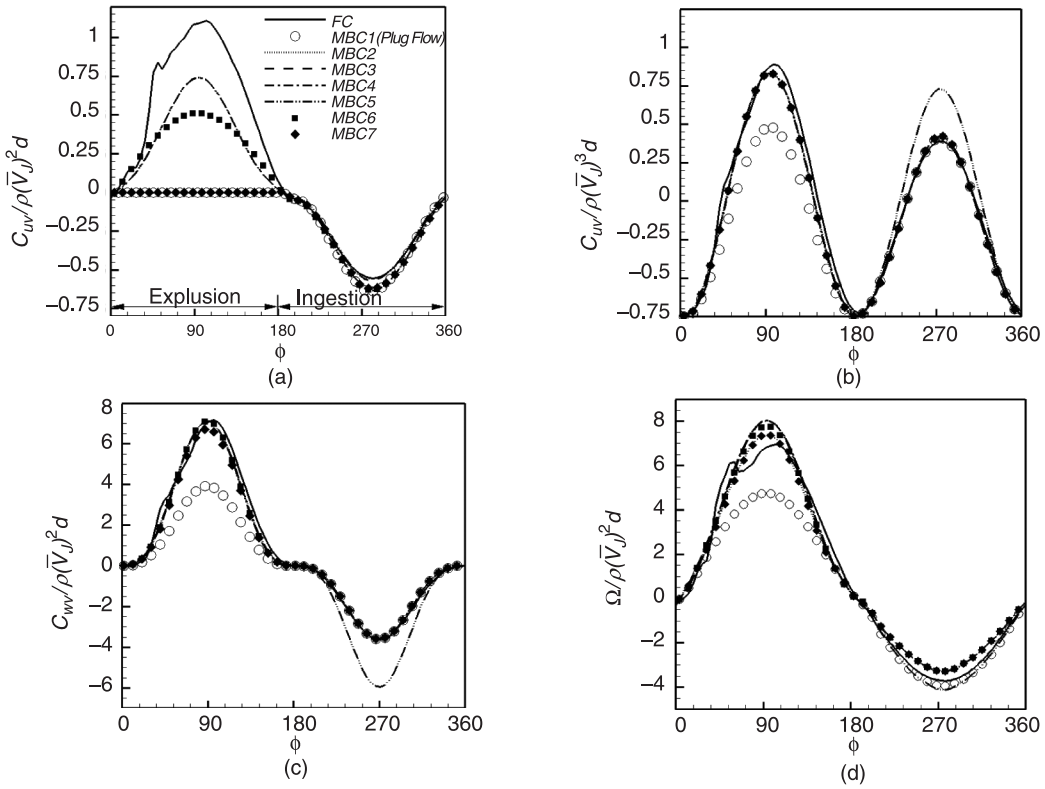

Figure 7: Comparison of the normalized instantaneous (a) u momentum flux, (b) v momentum flux, (c) vertical kinetic energy flux, and (d) spanwise vorticity flux for case with $\mathrm{Re}_J = 250$, $S = 7.07$, $St = 0.2$, $U_\infty/\overline{V_J} = 4$, and $\delta/d = 3$.

It is seen that the MBC1 (plug flow) model significantly underpredicts all four quantities during the expulsion phase, but there is a good agreement between this model and the full cavity model during the ingestion phase. One reason for this agreement might that the slot acts like a sink during the ingestion phase and sucks the flow from a semi-infinite medium and using a plug flow profile provides a good approximation to this flow. MBC2 and MBC3 overpredict the v momentum and vertical kinetic energy flux in the ingestion phase, which means that the two-degree of freedom profile is not a good candidate during the ingestion phase. As expected, the u momentum flux for MBC2 and MBC7 is zero due to zero u component of velocity in the expulsion phase. It should also be noted that in general, the horizontal momentum flux is significantly smaller than the flux of vertical momentum. MBC5 has the same performance as MBC4, even though the mean v-velocity V_0 has been neglected in this model. Comparing the MBC6 and MBC5 cases shows that neglecting the unsteady part of the u-velocity does not have a significant effect on these quantities and the u momentum flux is only slightly underprediced.

Table 2: Dimensionless time-average *u* momentum, *v* momentum, vertical kinetic energy and spanwise vorticity flux from jet during the expulsion and ingestion phases.

	$\frac{\overline{C_{uv}}}{\rho\left(\overline{V_J}\right)^2 d}$		$\frac{\overline{C_{vv}}}{\rho\left(\overline{V_J}\right)^2 d}$		$\frac{\overline{C_{vvv}}}{\rho\left(\overline{V_J}\right)^3 d}$		$\frac{\Omega}{\left(\overline{V_J}\right)^2}$	
	Expulsion	**Ingestion**	**Expulsion**	**Ingestion**	**Expulsion**	**Ingestion**	**Expulsion**	**Ingestion**
FC	**0.156**	**–0.058**	**0.416**	**0.286**	**0.785**	**–0.386**	**4.016**	**–2.375**
MBC1 (plug flow)	0.0	–0.061	0.305	0.287	0.406	–0.371	2.805	–2.737
MBC2	0.0	–0.057	0.391	0.352	0.751	–0.594	3.909	–2.452
MBC3	0.090	–0.057	0.391	0.352	0.751	–0.594	4.214	–2.455
MBC4	0.090	–0.060	0.391	0.287	0.751	–0.371	4.214	–2.730
MBC5	0.090	–0.061	0.386	0.287	0.738	–0.371	4.115	–2.737
MBC6	0.078	–0.061	0.386	0.287	0.738	–0.371	4.050	–2.737
MBC7	0.0	–0.061	0.386	0.287	0.738	–0.371	3.909	–2.737

Table 2 shows the dimensionless time-average of the flux of spanwise vorticity magnitude, *u* and *v* momentum flux, and vertical kinetic energy flux at the slot exit during the expulsion and ingestion phases. As expected MBC3 (the most complicated model), MBC4 and MBC5 most accurately predict the mean *u* momentum flux during the expulsion phase, whereas MBC1 (plug flow), MBC2, MBC7 significantly underpredict this quantity due to zero *u*-velocity for these models in this phase. The mean *v* momentum and vertical kinetic energy flux of all models except for MBC1 have good agreement with FC model over the expulsion phase, while MBC2 and MBC3 overpredict these quantities during the ingestion phase. All the models except MBC1 (plug flow) are able to estimate the time average of spanwise vorticity flux over the expulsion phase along the jet exit with reasonable accuracy.

Simulations have also been carried out for five other cases which include the following ranges of the parameters: $\mathrm{Re}_J = 125 - 250$, $S = 5 - 7.5$, $St = 0.133 - 0.45$, $U_\infty/\overline{V_J} = 4 - 8$ and $\delta/d = 3 - 6$ and the results for these are consistent with those for the case described in detail in the preceding discussion. Based on these observations, we select three models: MBC1, MBC6 and MBC7, for further analysis. Note that MBC1 is the simplest plug flow model with no unknowns. On the other hand, MBC6 and MBC7 are the simplest models with nonuniform expulsion velocities. Among these two, MBC6 model has two unknown parameters (U_0 and $V_1^{(3)}/V_1^{(2)}$) and MBC7 has only one unknown ($V_1^{(3)}/V_1^{(2)}$) parameter that requires closure.

The performance of these selected models is examined further by calculating the *u* momentum, *v* momentum and vorticity flux within the boundary layer at a downstream distance of 2*d* from the actuator. The objective here is to understand the extent to which the various models are able to match the downstream evolution of the disturbance produced in the attached boundary by the ZNMF perturbation. In Fig. 8 we show these non-dimensionalized integral quantities over the full duration of one expulsion cycle. It is seen that MBC1 is not able to capture the peak values of these quantities during the phase where the expelled vortices convect through the region of interest. On the other hand,

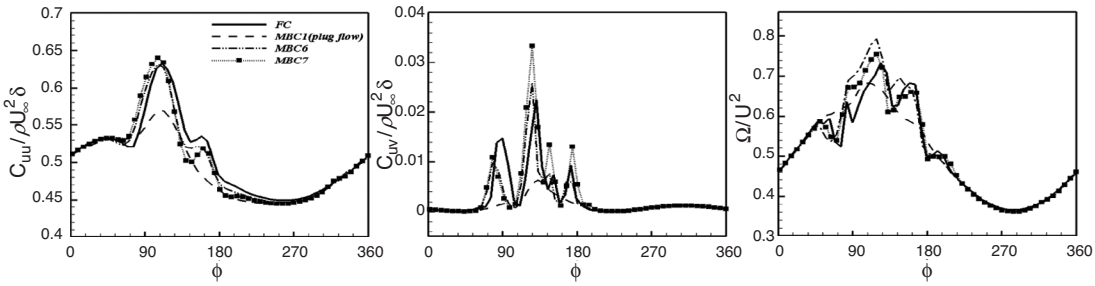

Figure 8: Comparison of *u* momentum (left), *v* momentum (middle) and vorticity flux (right) for selected models within the external boundary layer evaluated at 2*d* downstream of actuator over one cycle for $\mathrm{Re}_J = 187.5$, $U_\infty/\overline{V_J} = 4$, $\delta/d = 3$, $S = 7.5$, $St = 0.3$.

both MBC6 and MBC7 are able predict both the qualitative as well as quantitative features observed in the temporal variation of these quantities. We therefore expect that these two models will do a better job in reproducing the effect of the ZNMF jet on a downstream separation bubble and this issue is examined in the following section.

Model Performance for a Canonical Separated Flow

From a practical point-of-view in the context of separation control, the most important measure of fidelity of a model is the extent to which it matches the true effect of the ZNMF jet on a downstream separation bubble. We have examined this issue by simulating the case described in section II.B. Figure 9 shows the unsteady separation bubble formed by applying a steady suction and blowing on the top boundary, downstream of actuator for two cases $\mathrm{Re}_\delta = 2250$ and $\mathrm{Re}_\delta = 3000$. The adverse pressure gradient due to the suction on the top boundary reduces the momentum of the flow and eventually leads to boundary layer separation. The length of the separation bubble based on the mean flow shown by the streamlines in the figure are 41.8 d and 41.9 d for $\mathrm{Re}_\delta = 2250$ and $\mathrm{Re}_\delta = 3000$, respectively.

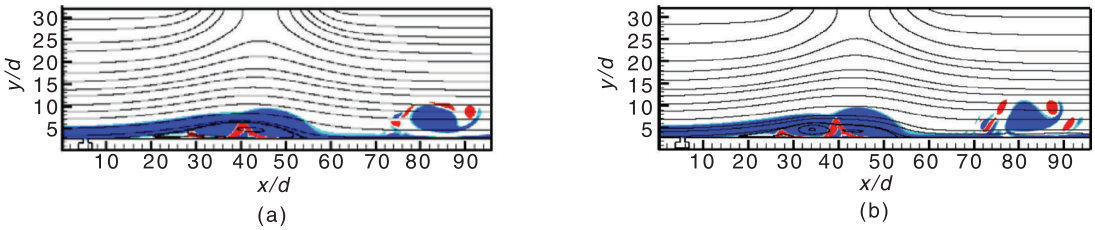

Figure 9: Instantaneous spanwise vorticity and mean streamlines for the unforced separated flow condition for (a) $\mathrm{Re}_\delta = 2250$ and (b) $\mathrm{Re}_\delta = 3000$.

The performance of the selected models MBC1, MBC6 and MBC7, in this canonical separated flow has been compared with the FC model in Fig. 10. The dimensionless flow parameters are $U_\infty/\overline{V_J} = 4$, $\delta/d = 3$, $\mathrm{Re}_J = 187.5$ with forcing frequency $F^+ = 1.0$. This figure shows the mean streamlines in the vicinity of the separation bubble for this flow condition. It is clear that MBC1 model is not able to capture the secondary separation bubble near the flow detachment point, while the MBC6 and MBC7 models are able to reproduce this feature. It is also seen that the MBC1 model cannot predict the detachment and reattachment of the flow accurately, whereas the location of these points by using MBC6 and MBC7 models are well matched with the FC model. A comparison between the maximum separation bubble height for the MBC's models and FC model shows that MBC1 significantly underpredicts this quantity, whereas the two other models provide a reasonable prediction of this quantity. One reason for this might be that the v momentum flux for MBC1 (plug flow) at the jet exit is less than the FC model during the expulsion phase.

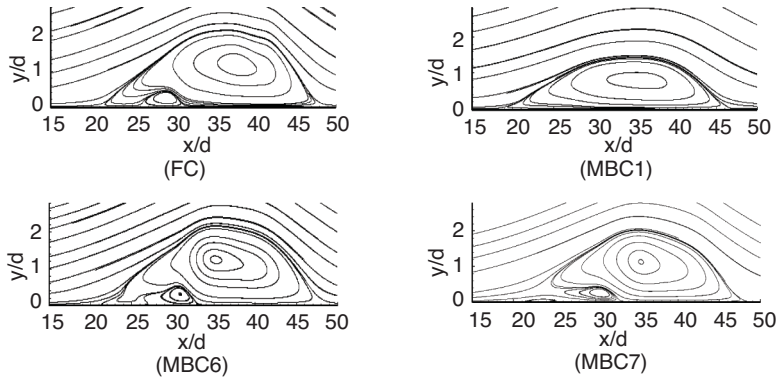

Figure 10: Mean streamlines of separated flow for $U_\infty/\overline{V_J} = 4$, $\delta/d = 3$, $\mathrm{Re}_J = 187.5$, $F^+ = 1.0$.

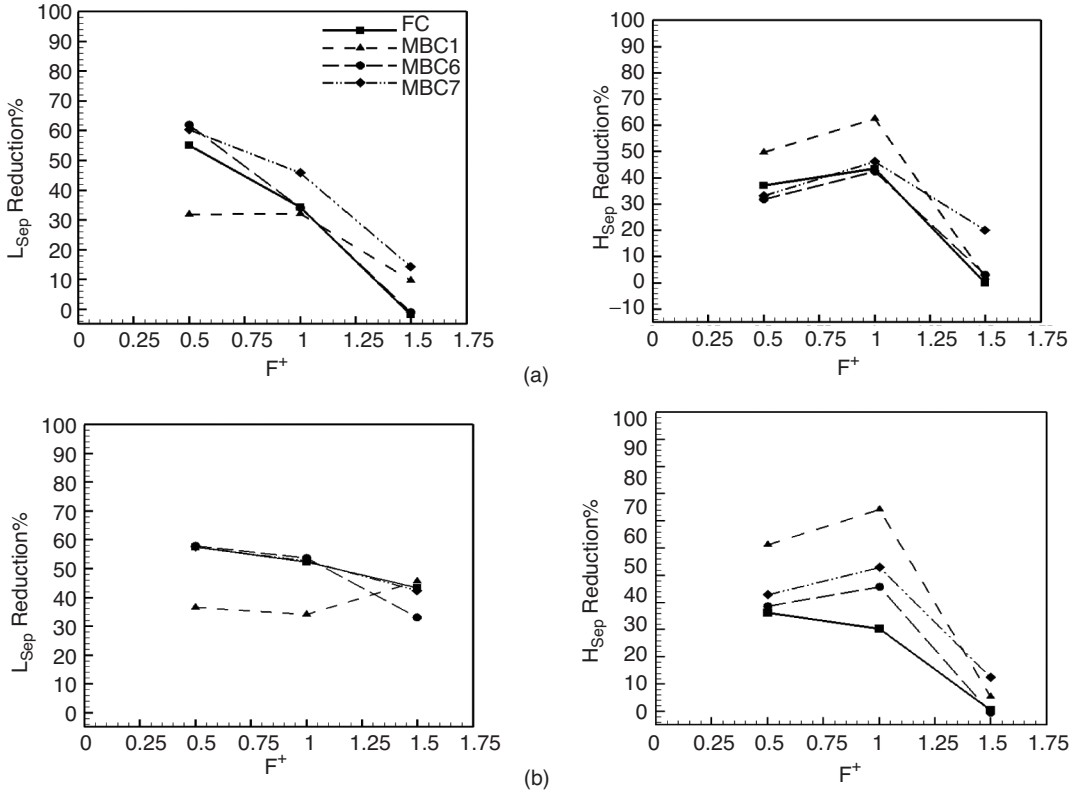

Figure 11: Effect of different forcing frequencies on the separation bubble length and height using FC, MBC1, MBC6 and MBC7 models in (a) $Re_J = 187.5$, (b) $Re_J = 250$.

Figure 11 summarizes the effect of selected models on the length and height of separation bubble for three forcing frequencies ($F^+ = 0.5, 1.0, 1.5$) and two jet Reynolds numbers $Re_J = 187.5, 250$. It is seen that in low forcing frequencies ($f_J < f_{Sep}$), where the actuator is effective in reducing the separation bubble, MBC6 and MBC7 models show good agreement with the FC model. On the other hand, the MBC1 underestimates the separation bubble length and overestimates separation height at low forcing frequencies. Furthermore, whereas MBC6 and MBC7 always correctly predict the trend of separation reduction with F^+, MBC1 actually predicts an incorrect trend of change in L_{Sep} with F^+ for both cases.

Model Closure

The above analysis has identified two models (MBC6 and MBC7) which are relatively simple, and which provide a reasonable improvement in fidelity over the plug-flow MBC1 model. However, both of these models have unknown parameters (U_0 and $V_1^{(3)}/V_1^{(2)}$) that need to be determined a-priori for a given flow configuration in order to be used in a predictive manner in any simulation. In general, these unknown parameters depend on the external flow as well as jet flow properties:

$$U_0 / \overline{V_J}, V_1^{(3)} / V_1^{(2)} = f(U_\infty / \overline{V_J}, \delta / d, S, \mathrm{Re}_J, ...) \tag{15}$$

and the above dependence is quite difficult to determine a-priori. Here we take a phenomenological approach to model closure. It is clear that the jet asymmetry (quantified by $V_1^{(3)}/V_1^{(2)}$ or alternatively by $\overline{V_J^R} / \overline{V_J^L}$) and slip (U_0) should depend on the grazing flow velocity upstream of the jet relative to the jet velocity. A measure of the local grazing flow velocity can be obtained from the available boundary layer velocity profile upstream of the jet. Alternatively, any simulation with flow control typically has a "baseline" case with no flow control and this grazing flow velocity could be extracted from this baseline simulation. While there are many possible ways of defining this velocity, a simple way is to associate this velocity with the streamwise velocity at a distance of 'd'

from wall upstream of the jet. We denote this velocity as U_d. Note that for the current Blasius boundary layer

$$\frac{U_d}{U_\infty} = \frac{3}{2}\frac{d}{\delta} - \frac{1}{2}\left(\frac{d}{\delta}\right)^3 \tag{16}$$

and therefore

$$\frac{U_d}{\overline{V_J}} = \frac{U_\infty}{\overline{V_J}}\left[\frac{3}{2}\frac{d}{\delta} - \frac{1}{2}\left(\frac{d}{\delta}\right)^3\right] = f\left(\frac{U_\infty}{\overline{V_J}}, \frac{\delta}{d}\right) \tag{17}$$

Based on our reasoning, ($\overline{V_J^R}/\overline{V_J^L}$) and slip ($U_0$) should depend primarily on $U_d/\overline{V_J}$ and we check this by extracting data from a sequence of simulations. Twelve separate ZNMF jet simulations with the following range of parameters have been carried out: $\mathrm{Re}_J = 125 - 375$, $S = 5 - 10$, $St = 0.133 - 0.533$, $U_\infty/\overline{V_J} = 1 - 8$ and $\delta/d = 3 - 6$. In addition, we have also carried out twelve steady jet simulations with these same parameters (these correspond to $St = S = 0$) in order to examine the extent to which the unsteadiness of the jet impact the above scaling.

The time average of the unknown parameters evaluated from the steady and unsteady jet for different $U_\infty/\overline{V_J}$ and δ/d, and fixed Re_J and St number are compared in Fig. 12. Interestingly, there is a fairly good agreement between the ZNMF and steady jets indicating that the physical processes that lead to jet asymmetry and slip are not intrinsically unsteady.

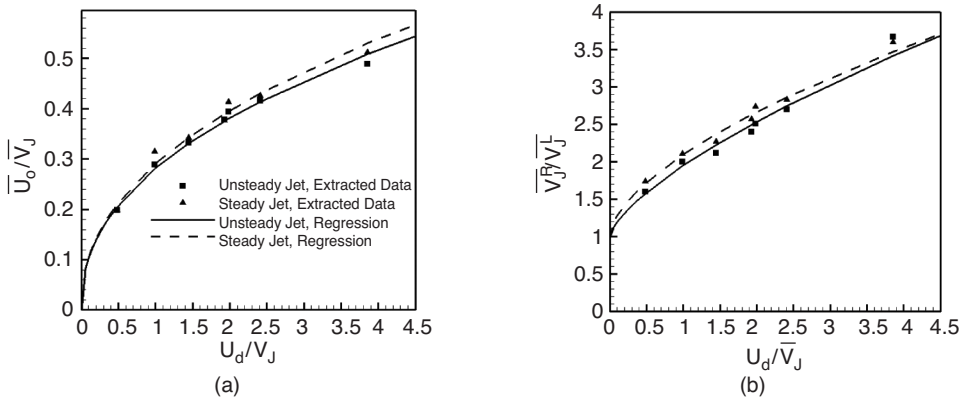

Figure 12: Comparison between the steady and unsteady jet for time average of (a) *u*-velocity and (b) *v*-velocity ratio along the slot exit for different $U_\infty/\overline{V_J}$ and δ/d. Re_J and St are fixed to 187.5 and 0.3 respectively.

We now use regression (least-squares fit) to determine an empirical power-law dependence of asymmetry and slip on $U_d/\overline{V_J}$. In conducting the regression analysis, we have also imposed the following limiting condition that applies for a jet in quiescent flow:

$$\lim_{U_\infty/\overline{V_J}\to 0} \frac{\overline{U_0}}{\overline{V_J}} \to 0 \qquad \& \qquad \lim_{U_\infty/\overline{V_J}\to 0} \frac{\overline{V_J^R}}{\overline{V_J^L}} \to 1 \tag{18}$$

The regression leads to the following expression for the steady and unsteady jets respectively:

$$\frac{\overline{U_0}}{\overline{V_J}} = 0.3\times\left(\frac{U_d}{\overline{V_J}}\right)^{0.45}; \qquad \frac{\overline{V_J^R}}{\overline{V_J^L}} = 1 + 1.1\times\left(\frac{U_d}{\overline{V_J}}\right)^{0.6} \tag{19}$$

$$\frac{\overline{U_0}}{\overline{V_J}} = 0.3 \times \left(\frac{U_d}{\overline{V_J}} \right)^{0.44}; \qquad \frac{\overline{V_J^R}}{\overline{V_J^L}} = 1 + 1.0 \times \left(\frac{U_d}{\overline{V_J}} \right)^{0.7} \tag{20}$$

It is also of interest to examine the dependence of the jet asymmetry and slip on the jet Strouhal and Reynolds numbers. Figure 13(a) compares the mean value of these two parameters for steady and unsteady jet for three different *St* and fixed $U_\infty/\overline{V_J}$, δ/d and Re_J. It is clear from this plot that both values are fairly independent of the Strouhal number in the range of study. Figure 13(b) shows the effect of Re_J number on the unknown parameters for steady and unsteady jet where the rest of flow parameters are fixed. It is seen that $\overline{U_0}$ is nearly independent of jet Reynolds number for both steady and unsteady jets whereas $\overline{V_J^R}/\overline{V_J^L}$ has a weak dependence on the Reynolds number. Thus, based on the above analysis we propose the following general forms for the scaling of the jet slip and asymmetry parameters:

$$\begin{aligned} \frac{\overline{U_0}}{\overline{V_J}} &= A \times \left(\frac{U_d}{\overline{V_J}} \right)^{\beta} \\ \frac{\overline{V_J^R}}{\overline{V_J^L}} - 1 &= B \times \left(\frac{U_d}{\overline{V_J}} \right)^{\gamma} \mathrm{Re}_J^{\kappa} \end{aligned} \tag{21}$$

While we have found values for A, B, β and γ for our generic configuration, it is likely that there is some variation in these values for each different configuration. Furthermore, turbulence in the grazing boundary layer might also modify the dependence, since ingestion of a turbulent flow by the actuator might change the flow pattern inside the slot and cavity and eventually of the jet coming out of the slot. Nevertheless, given that the above scaling laws seem to apply to unsteady as well as steady jets implies that the scaling approach is quite robust in representing the essential flow physics and would therefore be widely applicable. Furthermore, the approach described here might be directly applicable for the mean flow component of a turbulent flow as in a Reynolds-averaged Navier-Stokes (RANS) simulation.

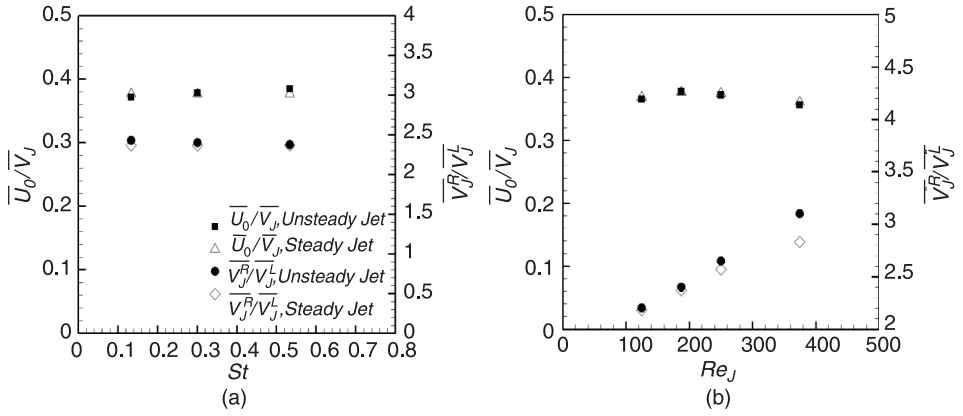

Figure 13: Comparison between the steady and unsteady jet for time average of *u*-velocity and v-velocity ratio along the slot exit for (a) different *St* number, fixed $U_\infty/\overline{V_J} = 4$, $\delta/d = 3$ and $\mathrm{Re}_J = 187.5$ and (b) different Re_J number, fixed $U_\infty/\overline{V_J} = 4$, $\delta/d = 3$, and $S_t = 0.3$.

IV. CONCLUSIONS

A class of modified boundary condition models is proposed to reproduce the flow associated with ZNMF jets in grazing flows. The proposed models have a nonuniform jet velocity profile with only two spatial degrees of freedom and a uniform slip velocity on the slot-flow boundary. A comparison of key integral quantities associated with momentum, energy and vorticity flux shows that the models with nonuniform jet velocity during the expulsion phase and uniform jet velocity during the ingestion phase can predict these quantities with good accuracy, whereas a simple plug flow model with zero slip and uniform jet velocity underpredicts these three quantities during the expulsion phase.

Based on our initial analysis, three of the simplest models were selected for further study, including an assessment of their performance for a canonical separated flow at different forcing frequencies. A key finding of this study is that a simple plug-flow type model can predict incorrect trends for separation reduction with jet frequency. Thus caution needs to be exercised in using such simple models in computational studies of flow control. It is also found that inclusion of a jet flow asymmetry parameter improves the fidelity of the model significantly and leads to better qualitative and quantitative prediction of separation control. Inclusion of a non-zero slip velocity improves the prediction of horizontal momentum flux from the jet but does not significantly improve the fidelity of the model.

A preliminary attempt has been made to provide empirical closure to the above models. Our simulations suggest that the two parameters in the models: jet asymmetry and slip, are well represented through a power law dependence on a parameter that quantifies the grazing flow velocity of the boundary layer upstream of the jet relative to the jet velocity. This parameter can be determined concurrently from a flow control simulation and the jet asymmetry model adjusted during the course of the simulation. Alternatively this quantity might be available from a baseline flow simulation (with no flow control) or from a potential flow type model of the configuration under consideration. The jet asymmetry also shows a weak power law dependence on the jet Reynolds number. Further analysis of these scaling laws and the extent to which they are universal needs to be investigates through additional analysis and simulations.

ACKNOWLEDGEMENTS

The work presented here is supported by NASA under cooperative agreement NNX07AD94A, monitored by Dr. Brian Allan. Partial support from AFOSR grant FA9550-09-1-0257 is also acknowledged.

REFERENCES

1. Seifert, A., Bachar, T., Koss, D., Shepshelovich, M., and Wygnanski, I., "Oscillatory Blowing: A Tool to Delay Boundary-Layer Separation," *AIAA Journal*, Vol. 31, No. 11, 1993, pp. 2052–2060.
2. Wang, H., and Menon, S., "Fuel-Air Mixing Enhancement by Synthetic Microjets," *AIAA Journal*, Vol. 39, No. 12, 2001, pp. 2308–2319.
3. Mahalingam, R., and Glezer, A., "Design and Thermal Characteristics of a Synthetic Jet Ejector Heat Sink," *Journal of Electronic Packaging*, Vol. 127(2), 2005, pp. 172–177.
4. Smith, B. L., and Glezer, A., "Jet Vectoring using Synthetic Jets," *Journal of Fluid Mechanics*, Vol. 458, 2002, pp. 1–24.
5. Gallas, Q., Holman, R., Nishida, T., Carroll, B., Sheplak, M., and Cattafesta, L., "Lumped Element Modeling of Piezoelectric-Driven Synthetic Jet Actuators," *AIAA Journal*, Vol. 41, No. 2, 2003, pp. 240–247.
6. Glezer, A., and Amitay, M., "Synthetic Jets," *Review of Fluid Mechanics*, Vol. 34, 2002, pp. 503–529.
7. Holman, R., Utturkar, Y., Mittal, R., Smith, B. L., and Cattafesta, L., "Formation Criterion for Synthetic Jets," *AIAA Journal*, Vol. 43, No. 10, 2005, pp. 2110–2116.
8. Raju, R., Aram, E., Mittal, R., and Cattafesta, L. N., "Simple Models of Zero-Net Mass-Flux Jets for Flow Control Simulations," *International Journal of Flow Control* , Vol. 1, No. 3, 2009.
9. Kral, L. D., Donovan, J. F., Cain, A. B., and Cary, A. W., "Numerical Simulation of Synthetic Jet Actuators," AIAA Paper 97-1824, 1997.
10. Rizzetta, D. P., Visbal, M. R., and Stanek, M. J., "Numerical Investigation of Synthetic-Jet Flow Fields," AIAA Journal, Vol. 37, No. 8, 1999, pp. 919–927.
11. Filz, C., Lee, D., Orkwis, P. D., and Turner, M. G., "Modeling of Two Dimensional directed Synthetic Jets using Neural Network-based Detereministic Source Terms," AIAA Paper 2003-3456, 2003.
12. Yamaleev, N. K., and Carpenter, M. H., "A Reduced-Order Model for Efficient Simulation of Synthetic Jet Actuators," NASA Technical Reports, NASA/TM-2003-212664, 2003.
13. Rathnasingham, R. and Breuer, K. S., "Coupled Fluid-Structural Characteristics of Actuators for Flow Control," *AIAA Journal*, Vol. 35, No. 5, 1997, pp. 832–837.

14. Agashe, J., Arnold, D. P., and Cattafesta, L., "Lumped Element Model for Electrodynamic Zero-Net Mass-Flux Actuators," AIAA Paper 2009-1308, January 2009.
15. Byrganhalli, R. R., "Numerical Study of Three Dimensional Synthetic Jets in Quiescent and External Grazing Flows," D.Sc. Thesis, 2007, Mechanical and Aerospace Engineering, The George Washington University, Washington, DC.
16. Tang, H., Zhong, S., Jabbal, M., Garcillan, L., Guo, F., Wood, N. J., and Warsop, C., "Towards the Design of Synthetic-Jet Actuators for Full-Scale Flight Conditions. Part 2: Low-dimensional Atuator Prediction Models and Actuator Design Methods," *Flow, Turbulence and Combustion*, Vol. 78, No. 3, 2007, pp. 309–329.
17. Utturkar, Y., Mittal, R., Rampungoon, P., and Cattafesta, L., "Sensitivity of Synthetic Jets to the Design of the Jet Cavity," AIAA Paper 2002–0124.
18. Raju, R., "Scaling Laws and Separation Control Strategies for Zero-Net Mass-Flux Actuators," D.Sc. Thesis, 2008, Mechanical and Aerospace Engineering, The George Washington University, Washington, DC.
19. Kotapati, R. B., Mittal, R., and Cattafesta, L. N., "Numerical Study of Transitional Synthetic Jet in Quiescent External Flow," *Journal of Fluid Mechanics*, Vol. 581, 2007, pp. 287–321.
20. Mittal, R., Dong, H., Bozkurttas, M., Najjar, F., Vargas, A., and Loebbecke, A., "A Versatile Immersed Boundary Method for Incompressible Flows with Complex Boundaries," *Journal of Computational Physics*, Vol. 227, No. 11, 2008, pp. 4825–4852.
21. Na, Y., and Moin, P., "Direct Numerical Simulation of a Separated Turbulent Boundary Layer," *Journal of Fluid Mechanics*, Vol. 370, 1998, pp. 175–201.